Mechanical Properties and Failure Mechanism of Resistance Spot Welding Joint of 0.13C – 6.98Mn Medium Manganese TRIP Steel

Yunming Zhu[a,b] [ID]*, Teng Liu[a], Yanfei Chen[a], Qunyi Yang[a,b], Xinxin Zhang[a,b], Zhengqiang Zhu[a,b]**

[a]Nanchang University, College of Advanced Manufacturing, Nanchang, China.
[b]Jiangxi Provincial Key Laboratory of Robot and Welding Automation, Jiangxi, China.

A single-pulse spot welding test was performed on 0.13C-6.98Mn medium manganese TRIP steel. The test results showed that the joint performance increases with a rise in welding heat input before splashing occurs. Owing to the fusion zone (FZ) being closest to the heat source, its austenite content was completely transformed and its performance was worse than that of the heat affected zone comprising austenite. The segregation bands of C and Mn observed in the FZ were considered to be the main reason for the deterioration of grain boundary strength. These characteristics of the weld zone led to evident intergranular cracking and transgranular fracture in the tensile test, and all samples in this test showed partial or complete interfacial fractures.

Keywords: *resistance spot welding, medium manganese TRIP steel, microstructure, fracture mechanism.*

1. Introduction

In recent years, the automobile industry has developed rapidly and car ownership has increased linearly, thereby causing intense pressure on the resources and environment. Energy conservation and emission reduction have become necessary conditions for vehicles. Lightweight characteristics are important for automobile energy saving and emission reduction. It has been reported that when vehicle weight is reduced by 10%, vehicle fuel consumption, fuel combustion, and CO_2 emissions would decrease by 6%–8%, 1 L, and 2.45 kg[1], respectively. Under this demand, third generation of advanced high strength steel (AHSS) medium manganese TRIP steel is attractive and developed because of its combination of high strength and ductility[2-5]. The comprehensive mechanical properties of the third generation of AHSS are superior than those of the first generation of AHSS and equivalent to those of the second generation of AHSS; however, its cost is far lower than that of the second generation of AHSS, rendering it more advantageous as a manufacturing material in the future[6]. Moreover, through the TRIP effect of austenite, the steel strength can be increased to 800–1000 MPa. The third generation of automobile steel exhibits the same strength, while having a lighter weight; the elongation after fracture can reach 50–80%, and the strength-plastic product was 50–70 GPa·%. It exhibits a better energy absorption effect in the deformation process, and its performance meets the plastic requirements of automobile steel[7,8].

Since the application of medium manganese TRIP steel in automobile bodies is still in its infancy, the research on its weldability is extremely valuable. Cunyu Wang et al.[9] questioned the weldability of medium manganese steel due to its high carbon equivalent. In order to verify its weldability, 0.1C-5Mn medium manganese steel and high-strength galvanized H340LAD + Z steel were welded by dissimilar resistance spot welding. Surprisingly,

it was found that there was no defect in the cross section of the nugget, which met the requirements of the automobile factory. However, the carbon equivalent of medium manganese steel studied was as high as 0.9, and the same resistance spot welding of medium manganese steel was not carried out. Finally, it was pointed out that it was necessary to systematically study the spot welding between medium manganese steel. Jia et al.[10] reported that in spot welding of 5Mn steel, even if enough heat was input during welding to cause serious overflow, the expected form of PF fracture could not be produced. Wang et al.[11,12] tried to change the IF mode to PIF in the CT test of spot-welded 7Mn steel by adjusting the cooling time after welding and the heating pulse after welding, which was attributed to the high toughness of tempered martensite prevention of crack propagation in the nugget. However, there is no explanation in the study on how cracks in tempered martensite propagate first along the interface of the two welding plates, and then propagate perpendicular to the interface.

In this study, quasi-static tensile test, microhardness test, field emission scanning electron microscopy, and X-ray diffraction (XRD) were used to analyze the microstructure, phase transformation process, and failure mechanism of spot welding joints along with the segregation behavior of the main alloying elements. The purpose is to analyze the embrittlement reason and crack propagation path of the spot welding joint of medium manganese TRIP steel.

2. Materials and Methods

The medium manganese TRIP steel used in this experiment is a 1.6 mm cold rolled steel plate produced by Shanghai Baosteel. The microstructure of the base metal (BM) of the material at room temperature exhibits a ferrite + austenite dual phase structure. Table 1 shows the chemical

*e-mail: zhuzhq01@126.com

composition of 0.13C-6.98Mn medium manganese TRIP steel. During deformation, retained austenite induces martensitic transformation (namely TRIP effect) and thus achieves high strength and superior ductility[13,14]. Therefore, it exhibits high applicability in manufacturing lightweight vehicle bodies.

The MDZ-200 Intermediate Frequency Inverter Spot Welding Machine was used for resistance spot welding (RSW). Based on to the welding specification of a 1.6 mm thin plate according to the ISO18278-2016 standard, the electrode cap comprised an electrode made of chromium-zirconium-copper alloy with an end face diameter of 8 mm. Subsequently, an optimized welding process with single-pulse current (1 cyc = 0.02 s) was designed, as shown in Figure 1a. Preloading time and holding time were 600 ms and 300 ms, respectively; electrode pressure was 4 kN; welding time was 320 ms; and welding current increased from 8 kA to 12 kA.

The metallographic specimens were etched in a 1% nitric acid aqueous solution, and the microstructure was characterized using an optical microscope (German Kaercaisi, model: Axioscope.A1) and a scanning electron microscope (SEM; German Kaercaisi, model: AURIGA). The element content and distribution in different structural zones of the weld were tracked using the SEM and the point scanning, line scanning, and surface scanning functions of the energy dispersive spectrometer (EDS). Further, the effects of different phases and element distribution behaviors on the stability of austenite and the grain size of the martensite

phase morphology were investigated. The samples were analyzed via XRD (copper α radiation, 35 kV, 150 uA, Brook D8 Discover, Germany), and the volume fraction of residual austenite was calculated using Formula 1[15]:

$$V_A = \frac{1.4I_\gamma}{I_\alpha + 1.4I_\gamma} \tag{1}$$

Among them, V_A represents the austenite volume fraction; I_γ is the integral strength of the diffraction peaks of austenite crystal planes (200), (220), and (311); and I_α is the integral strength of the diffraction peaks of ferrite crystal planes (200) and (221).

The Vickers hardness tester (model: Durascan-70) was used to evaluate the microhardness. The pressure was set at 300 g and the holding time was 15 s. Vickers hardness distribution of base metal, heat affected zone and fusion zone was measured by microhardness tester, and hardness variation was analyzed to characterize the overall strength of the material. A quasi-static tensile test was implemented by using the Instron5982 electronic universal testing machine, with a maximum load of 100 kN. According to the ISO14273-216 standard, the specimen dimensions for the tensile shear test at room temperature should be 135 mm × 60 mm, while the beam displacement velocity is 2 mm/min. Figure 1b shows the tensile specimen size used in this test.

Table 1. Chemical composition of 0.13C-6.98Mn experimental steel (Wt %).

| C	Si	Mn	P	S	Cr	Ni	Al
0.13	0.22	6.98	0.006	0.0011	0.09	0.10	0.04
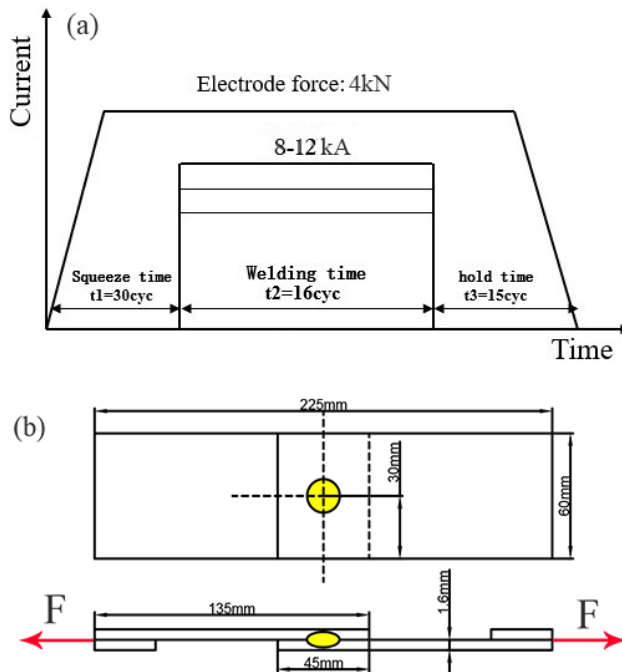
Figure 1. (a) Single-pulse welding process; (b) schematic diagram of weld microhardness test; (c) tension and shear specimen.

Mechanical Properties and Failure Mechanism of Resistance Spot Welding Joint of 0.13C – 6.98Mn Medium Manganese TRIP Steel

3

3. Results and Discussion

3.1. Microstructure evolution

The matrix of medium manganese TRIP steel is generally composed of face-centered cubic structure of retained austenite and body-centered cubic structure of ferrite[16-18]. Martensitic transformation (A → M) tends to occur during the rapid cooling process after welding. The macroscopic morphology and microstructure of the weld zone of Fe-0.13C-6.98Mn medium manganese TRIP steel are given in Figure 2. Similar
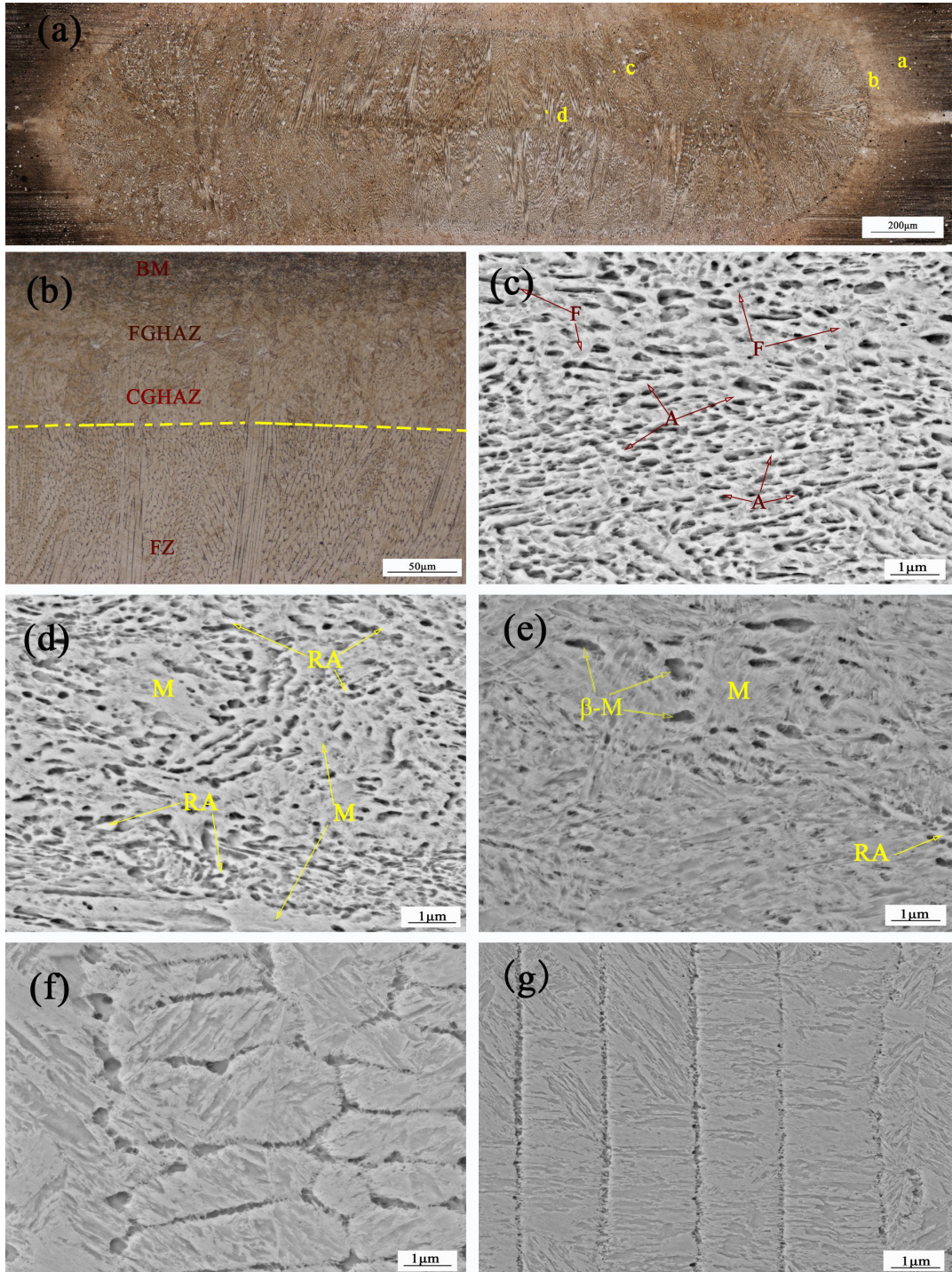
Figure 2. Macromorphology and microstructure of nugget in Fe-0.13C-7Mn TRIP steel: (a) macromorphology of nugget; (b) tissue evolution from base metal to fusion zone. Structures of the (c) heat affected zone, (d) fine grain heat affected zone, (e) coarse grain heat affected zone, and ((f) and (g)) fusion zone martensite.

to most resistance spot welding joints[19-21], the spot-welding joints of medium manganese TRIP steel mainly have three structural zones: BM, heat affected zone (HAZ), and FZ. Figure 2b shows that from the BM to the FZ, the grains in HAZ near the BM are relatively fine, while the grains near the FZ are relatively coarse. Therefore, it can be divided into the FGHAZ and CGHAZ. The difference in grain size between the two zones is mainly affected by heat input and high temperature residence time. Owing to the influence of the temperature gradient, the columnar grains at the boundary of the FZ were basically perpendicular to the fusion core line, which is similar to the conclusion of Yuan et al.[22].

After the solidification and crystallization of the weld, the phase transformation process of the internal microstructure also concluded. Points a, b, c, and d in Figure 2a correspond to the FGHAZ (Figure 2d), CGHAZ (Figure 2e), FZ (Figure 2f), and nugget center zone (Figure 2g), respectively. It can be seen from Figure 2d and Figure 2e that martensite (M) and ferrite (F) are distributed in the fine-grained and coarse-grained regions of the HAZ, a small amount of tempered martensite(β-M) was found in the coarse grained region (Figure 2e) and there are small amounts of residual austenite in the edge regions of martensite and ferrite. The retained austenite content in the fine grain region near the BM is significantly more than that in the coarse grain region (austenite is almost completely transformed). Because the fine grain region was far away from the welding heat source, some tissues were not heated up to the austenite transformation temperature line and left to cool; therefore, the region retains more austenite, with the BM exhibiting fine grain characteristics and the toughness being relatively good. The cooling transformation process near the fusion line reaches Ms for a longer time because it remains closer to the heat source for a longer time; therefore, more austenite transformations are observed along with many coarse martensites and lath martensite substructures. The columnar crystals in the FZ are distributed with a large number of lath martensites (as shown in Figure 2f and Figure 2g).

Residue austenite is metastable phase, continuous transformation to martensite under stress can improve work hardening effect, thereby improving strength and plasticity of materials[23]. Figure 3 shows the residual austenite contents of the BM, HAZ, and FZ at the joint. It can be seen from the figure that the residual austenite content gradually decreases from BM to FZ. The residual austenite content

of BM is 26%, and the residual austenite content of HAZ is about 16%, However, it is difficult to detect the presence of trace austenite by XRD method, so the austenite in FZ is 0. Residual austenite decreases gradually from BM to FZ, which is similar to the conclusion of Jia et al.[10].

3.2. Element segregation

Austenite would transform to martensite when subjected to a thermal cycle and cooling after spot welding of medium manganese TRIP steel. It is generally believed that martensitic transformation is a non-diffusive transformation. The starting temperature of this transformation is Ms and the ending temperature is Mf. The activity of C and Mn atoms is related to temperature, and the phase transition rate is closely related to the initial temperature and the range of phase transition temperature. A higher initial transition temperature usually leads to relatively greater transition rates. However, Han et al.[24] concluded that the transformation amount of martensite gradually increased with the decrease of temperature. Therefore, it is of great significance to study the segregation behavior of major alloying elements such as C and Mn for elucidating martensitic transformation.

Figure 4 shows the EDS results for columnar crystal surfaces in the FZ. It can be clearly seen that the segregation band of Mn forms at the grain boundary, which hinders the lateral growth of the grain boundary. Furthermore, the temperature gradient in the vertical direction is large, and the grains grow continuously along the electrode direction to form slender columnar grains. The primary austenite growth is also inhibited; the martensite grain boundary cannot migrate during final cooling, which is interlaced in the middle of the segregation band. As a result, the mechanical properties of the nugget are uneven and brittle fracture occurs easily during tensile shear.

3.3. Mechanical properties analysis

The lap shear tensile test is used to qualitatively evaluate the mechanical stability of welded joints[25]. Previous studies have shown that the geometric size of spot weld nuggets is one of the most important factors affecting the mechanical properties of solder joints[26]. With an increase i nugget diameter, the comprehensive mechanical properties of solder joints show an increasing trend. Figure 5 shows the variation trends of the peak tension and nugget diameter for the spot welding joint with single-pulse current, time, and electrode
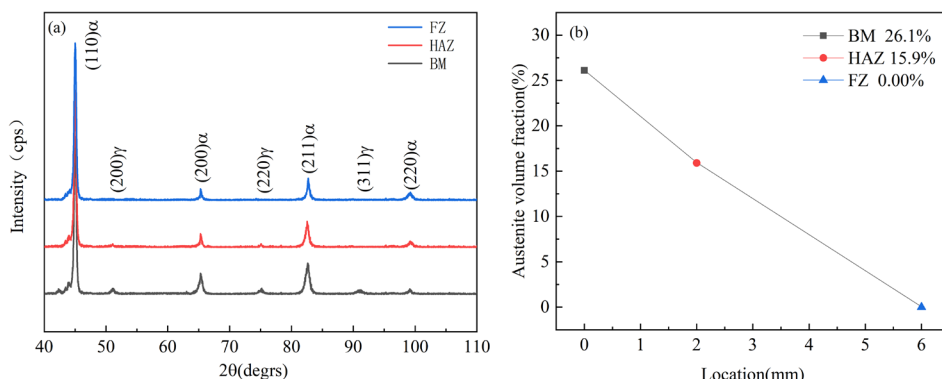
Figure 3. Residual austenite content at different locations of the joint: (a) X-ray diffraction pattern; (b) volume fraction of residual austenite.
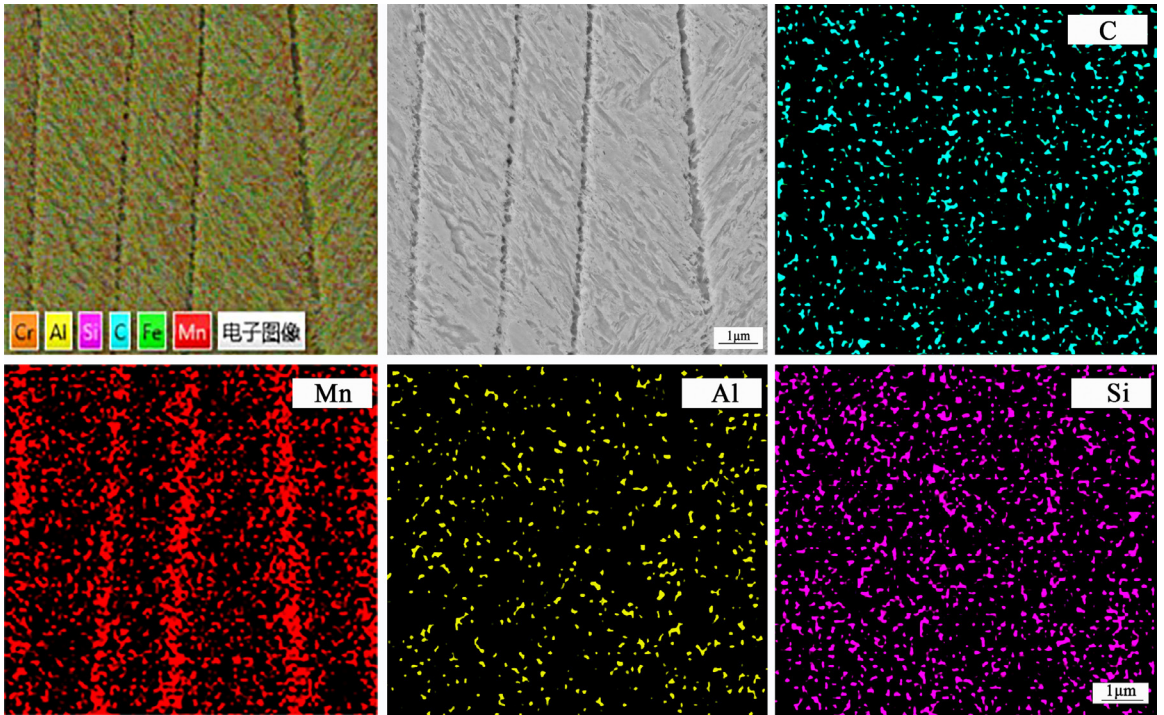
Figure 4. Scanning electron microscope images of microstructure and element distribution in the fusion zone.
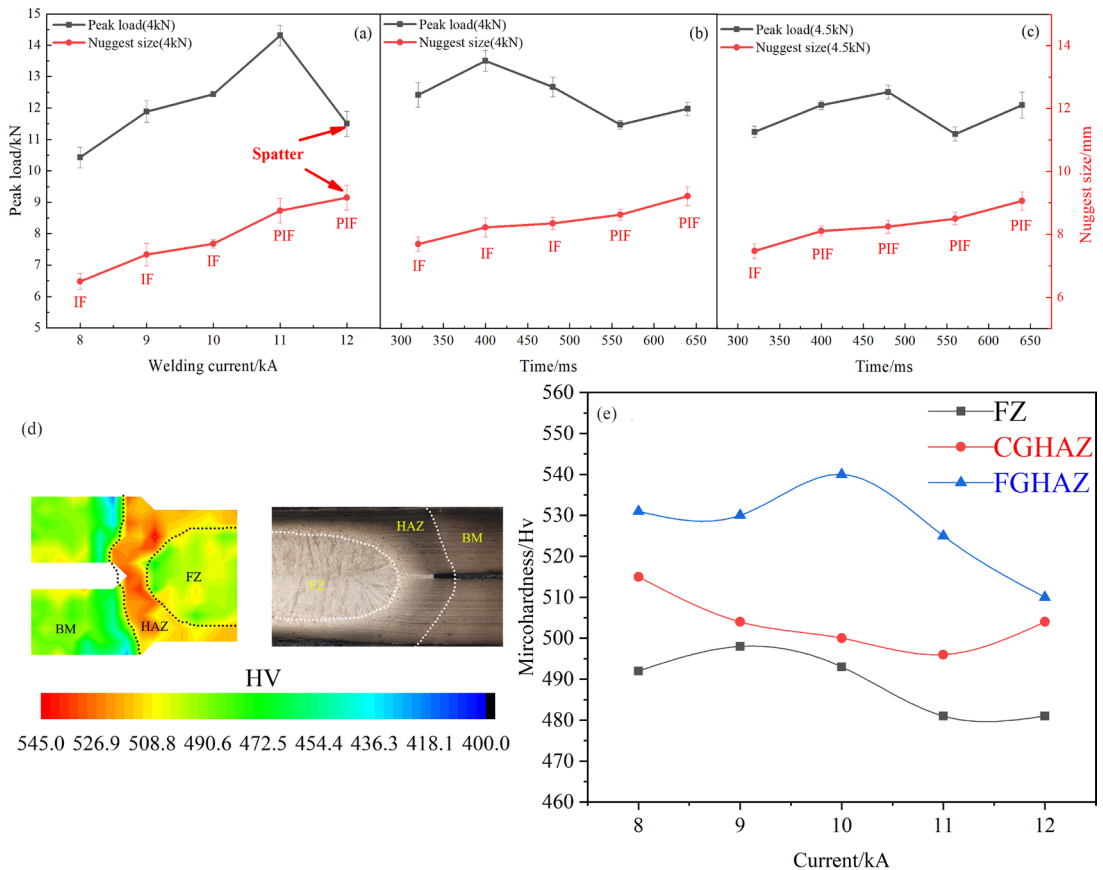

Figure 5. (a), (b), and (c) are the effects of welding current, welding time, and electrode force on peak load and nugget diameter, respectively; (d) microhardness distribution of solder joints at 10 kA; (e) hardness characteristics of each structural region of solder joint.

pressure. By comparing the effects of current (Figure 5a) and time (Figure 5b) on the mechanical properties of these joints, it can be found that the welding current of nugget diameter is proportional to time, and the peak tension appears a critical value. The fracture mode is proportional to the nugget diameter. When the nugget diameter is large enough, the transformation from IF to PIF occurs. When the current increased to 12 kA, a strong splash occurred. Although the nugget diameter (9.15 mm) increases slightly compared to that at 11 kA (8.73 mm), a part of the weld metal was lost due to the discharge of molten metal from the plastic ring under the action of the electrode pressure and the mechanical properties of the solder joint decreased significantly. When the welding time exceeds 400 ms, the peak load begins to decrease after reaching a maximum (13.5 kN); this can be attributed to the increase in welding time, which augmented the widths of the HAZ and coarse grain. This part of the coarse grain area is often regarded as sensitive in the failure test.

Comparing Figure 5b with Figure 5c reveals that when the electrode pressure increases to 4.5 kN and the welding time reaches 480 ms, the variation in the peak load becomes small and tends to stabilize, showing that it first increases rapidly and then slowly. In the short welding time range of 320–480 ms, the joint with a higher strength was obtained at a lower electrode pressure (maximum strength was achieved at 400 ms). In the welding time range of 480–640 ms, the welding joint subjected to a 4.5 kN electrode force was more reliable than that experiencing a 4 kN electrode force. This could be attributed to the fact that increasing the electrode pressure would augment the contact area between the electrode and the plate, rendering the total resistance and welding current smaller. Accordingly, the welding heat input is reduced according to the empirical formula Q = I2Rt; therefore, the nugget diameter of the spot welding joint under 4.5 kN is smaller and the peak load is lower than those under 4 kN.

Comparing the three figures in Figure 5 reveals that the welding current had the greatest influence on the mechanical properties of the spot welding joint. Although the welding time and electrode pressure also had influences on the tensile shear strength, there was no regular effect. The transformation of fracture mode has a great relationship with the nugget diameter, but has little relationship with the peak load, which is similar to the conclusion of Pouranvari[27,28]. No spatter was observed in experiments wherein peak tension and nugget diameter changed with welding time and electrode pressure. This indicates that the generation of splash is mainly affected by the welding current, which further implies that the welding current is the main factor affecting the mechanical properties of solder joints.

FZ of spot welding joint of medium manganese TRIP steel is mainly composed of martensite. It is reported that martensite hardness of steel with carbon content higher than 0.05% is higher than 350 Hv[29]. Figure 5d shows the hardness distribution at a welding current of 10 kA. The maximum microhardness of HAZ of 10 kA sample is 540 Hv, and the average microhardness is 520 Hv, followed by the average microhardness of FZ is 500 Hv, and the average microhardness of BM is 490 Hv. When the BM transitioned to the HAZ, the hardness increased sharply and there was no softening phenomenon. After transitioning to FZ, the hardness fluctuated to a certain extent. To verify whether the hardness of HAZ is

higher than that of other structural regions, the hardness of the FZ, fine grain heat affected zone (FGHAZ), and coarse grain heat affected zone (CGHAZ) of all samples within the welding parameters was tested; the results are shown in Figure 5e. When the welding current increases from 8 to 12 kA, the peak temperature of the welding thermal cycle also rises gradually. Meanwhile, the hardness of the FZ and CGHAZ in the range of 8–12 kA decreases, while that of the FGHAZ increases first and then decreases. Meanwhile, the decrease in the hardness of the fusion zone (FZ) from 8 to 11 kA mainly occurs due to the increase in the input amount, which led to the formation of a large grain during martensite transformation; the final transformation product was a coarse grain. Combining the peak load curve analysis of Figures 5a, b and c reveals that the mechanical properties of the weld increase with a decrease in the hardness of the FZ.

3.4. Fracture mode

In a tensile shear test, the failure modes of spot welding joints are generally divided into three types: IF, PIF, and PF[30]. Generally, the failure mode of spot welding is a competition between the interface failure load (F_{IF}) and the critical load (F_{PF}) at pullout failure. Failure modes can be distinguished using Formula 2[31]:

$$D_c = \frac{4t\sigma_{PFL}}{P\tau_{FZ}} \tag{2}$$

Where D_c is the critical nugget diameter, t is the plate thickness, P is the percentage of pores and shrinkage pores in the nugget ($0 < P \le 1$), σ_{PFL} is the ultimate tensile strength at the fracture position, and τ_{FZ} is the shear strength of nugget.

(1) When $F_{IF} < F_{PF}$, the shear stress in the nugget center preferentially reaches the critical failure load, resulting in shear deformation and eventually interface failure.

(2) When $F_{IF} > F_{PF}$, the tensile stress in the HAZ or the area near the BM preferentially reaches the critical failure load and produces necking, resulting in pull-out failure.

(3) In some special cases, the shear stress in the nugget center first reaches the critical value and the interface failure occurs. Subsequently, the crack grows in the FZ. As the crack further expands to the HAZ, the critical tensile stress decreases and then the pull-out failure occurs. The failure mode where IF and PF coexist is called PIF.

From the tensile-shear test results of the spot welding joint of 0.13C-6.98Mn medium manganese TRIP steel, it was observed that the fracture modes were mainly PIF and IF, no PF joint was obtained, and the crack propagation path was complex. The failure of solder joints can be summarized to exhibit three stages: crack initiation, crack propagation, and final instantaneous fracture.

The typical IF failure mode (4 kN, 320 ms, 9 kA samples) in the tensile-shear test of 0.13C-6.98Mn medium manganese TRIP steel is shown in Figure 6. Figure 6a shows the macroscopic crack propagation path, Figure 6b reveals the local ductile fracture morphology of strip grains near the fusion line, and Figure 6c demonstrates the amplification morphology of the macroscopic crack terminal. In the IF
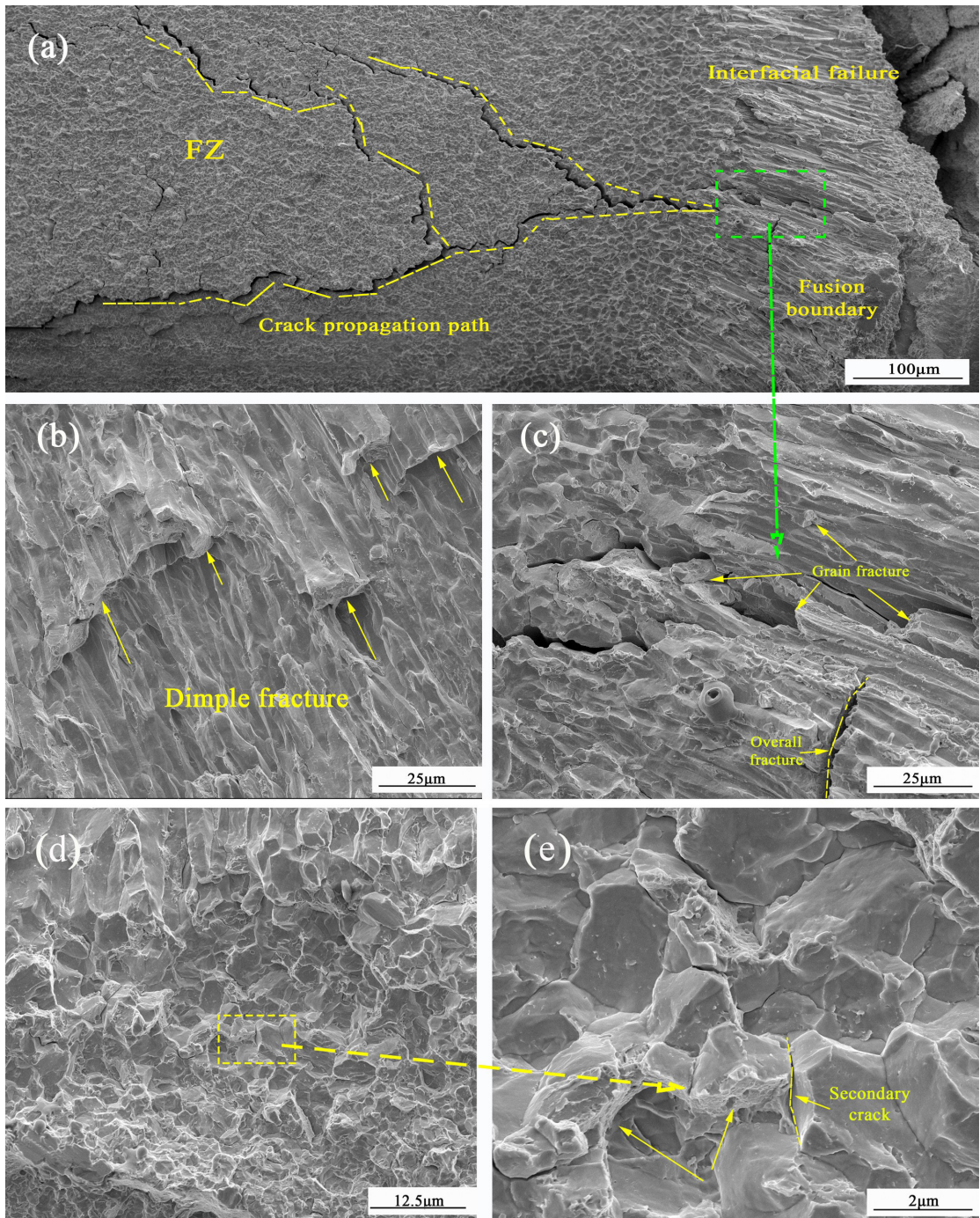
Figure 6. Fracture morphology corresponding to interface failure: (a) crack propagation path; (b) fracture morphology of nugget boundary; (c) crack terminal magnification; (d) fracture morphology of heat affected zone; (e) amplification morphology of frame-line area.

fracture mode, the macro-cracks are generally "V" shaped and comprise multiple branches. There are many small intergranular cracks around these macro-cracks, which generally represent the tensile shear force in the same direction. With further propagation of cracks, when the region near the fusion line is close, the branched cracks converge into the main cracks and continue to extend in the same direction until the solder joint completely breaks (green frame part in Figure 6a).

The grain morphology in the nugget center mainly comprises coarse blocks and dendrites, and the stress distribution at the grain boundary is very dense. Furthermore, there are many internal defects in the acicular martensite. When bearing external tensile stress, effective plastic deformation cannot occur; therefore, a typical brittle fracture is observed. The elongated columnar crystals near the fusion line (Figure 6b) show the fracture direction; many
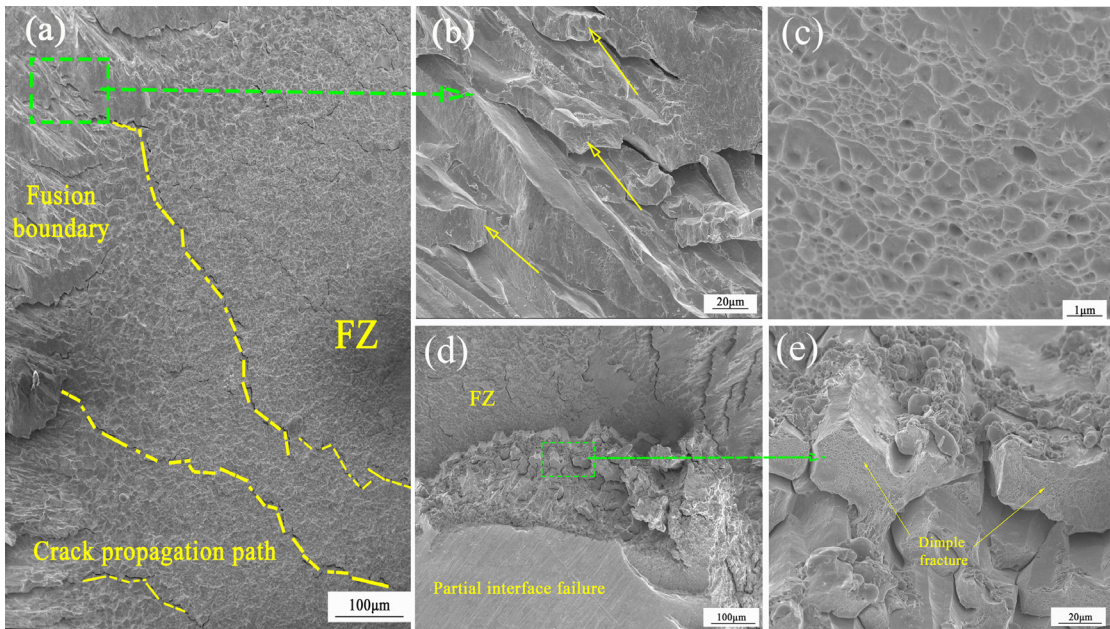
Figure 7. Fracture morphology of partial interface failure: (a) crack propagation path; (b) edge fracture in the fusion zone; (c) dimples in the arrow direction in Figure b; (d) macroscopic fracture; (e) amplification morphology of frame-line area.

shallow dimples can be observed at the fracture, which may indicate the self-tempering phenomenon of martensite lath. Therefore, this kind of grain has certain plasticity, and its bearing capacity is better than that of the microstructure in the core area. When the solder joint fails, it often breaks at the end. The CGHAZ microstructure near the fusion line mostly comprises irregular polygonal grains, which will deteriorate the mechanical properties in the region. In the loading process of tensile shear force, the fracture mode is almost the same as that of FZ, with split crystalline structures (Figure 6d) and secondary cracks being observed (Figure 6e). This part of the region and the FZ together constitute the brittle and sensitive area under the IF mode.

Figure 7 shows the typical fracture morphology associated with PIF (4 kN, 320 ms, 12 kA samples) for a single pulse test. Generally, the transformation of failure mode is usually related to the increase of nugget diameter[27,28]. Russo Spena et al.[32] concluded that the generation of PIF mode is caused by the high stress concentration of weld. Figure 7d and Figure 7e represent the parts above the FZ that do not exhibit interfacial fractures. A clear dimple distribution can be observed on the fracture surface of the grains broken in the central region of the nugget (Figure 7c). Such long columnar grains have a higher carrying capacity than that of the massive or lamellar grains around it; their stress distributions are also relatively uniform. However, no dimples are observed at the fracture interface between adjacent grains; therefore, they still exhibit brittle fracture in general. In addition to the grain size and morphology of the FZ affecting its strength and hardness characteristics, the hardness of the FZ and HAZ also has a significant impact on the fracture mode. The lattice distortion of acicular martensite with high hardness is large, and its existence will produce many high-density microcracks, which increase the tendency of brittle fracture of solder joints. More

cracks can be observed around the FZ perpendicular to the direction of the plate (Figure 7a), and the propagation paths of these cracks are similar to those of the IF mode; however, the crack terminal shows evident brittle fracture, and there are no ductile fractures with dimples at the edge of the fusion line. This part of the grain presents the phenomenon of lamellar tearing from the bottom up, which is connected with more cracks in the FZ (Figure 7b). Compared with the IF mode, the morphology at the interface between FZ and HAZ (Figure 6b) is more irregular, rougher, and does not show a fixed direction. Furthermore, the grains are mostly coarse lamellar structures, which significantly decrease tensile strength.

4. Conclusions

The mechanical properties, microstructure, and fracture behavior of the spot-welding joint of Fe-0.13C-6.98Mn-0.22Si medium manganese TRIP steel were studied. The main findings are as follows:

(1) In the single pulse test, the effects of welding current, welding time, and electrode pressure on the mechanical properties of solder joints, nugget nucleation, and size were studied. Under a given electrode pressure and before the occurrence of spattering, the larger the welding current and the longer the welding time, the greater the welding heat input; accordingly, the peak load and nugget diameter of the solder joint increase. The electrode pressure affect the energy density and distribution in the welding process. Increasing the electrode pressure can reduce the contact resistance and decrease the welding energy. It is found that the transformation of failure mode mainly depends on the fusion diameter, which has little relationship with the peak load.

(2) The microstructure of the HAZ in the spot-welding joint of 0.13C-6.98Mn medium manganese TRIP steel mainly comprised martensite, residual austenite, and ferrite. The FZ almost complexly exhibited a martensite structure, and the volume fraction of residual austenite decreased gradually from the BM to the FZ. The hardness test results showed that the hardness of the HAZ was the highest and that of the BM was the lowest. However, the local hardness decreased in the HAZ (CGHAZ), and the mechanical properties of the weld increased with the decrease in the hardness of the FZ.

(3) The surface scanning results of the FZ showed that the Mn segregation bands of the long columnar crystals hinder the grain boundary migration, resulting in the continuous growth of grains along the electrode direction. The enrichment of elements led to the deterioration of the intergranular strength.

(4) The fracture modes of the joint in single pulse test were IF and PIF. The IF mode mainly included intergranular fracture, while the PIF mode had a certain ductility; however, the intergranular brittleness was significant. The fracture behavior was determined by the nugget size.

5. Acknowledgments

6. References

1. Zhang Y, Lai X, Zhu P, Wang W. Lightweight design of automobile component using high strength steel based on dent resistance. Mater Des. 2006;27(1):64-8.

2. Merwin MJ. Low-carbon manganese TRIP steels. Mater Sci Forum. 2007;539:4327-32.

3. Suh DW, Park SJ, Lee TH, Oh C-S, Kim S-J. Influence of Al on the microstructural evolution and mechanical behavior of low-carbon, manganese transformation-induced-plasticity steel. Metall Mater Trans, A Phys Metall Mater Sci. 2010;41(2):397-408.

4. Lee S, Lee SJ, Santhosh Kumar S, Lee K, Cooman BCD. Localized deformation in multiphase, ultra-fine-grained 6 Pct Mn transformation-induced plasticity steel. Metall Mater Trans, A Phys Metall Mater Sci. 2011;42(12):3638-51.

5. Shi J, Sun X, Wang M, Hui W, Dong H, Cao W. Enhanced work-hardening behavior and mechanical properties in ultrafine-grained steels with large-fractioned metastable austenite. Scr Mater. 2010;63(8):815-8.

6. Cai ZH, Ding H, Xue X, Jiang J, Xin QB, Misra RDK. Significance of control of austenite stability and three-stage work-hardening behavior of an ultrahigh strength–high ductility combination transformation-induced plasticity steel. Scr Mater. 2013;68(11):865-8.

7. Frommeyer G, Brüx U, Neumann P. Supra-ductile and high-strength manganese-TRIP/TWIP steels for high energy absorption purposes. ISIJ Int. 2003;43(3):438-46.

8. Grässel O, Krüger L, Frommeyer G, Meyer LW. High strength Fe–Mn–(Al, Si) TRIP/TWIP steels development—properties-application. Int J Plast. 2000;16(10-11):1391-409.

9. Wang C, Li X, Han S, L Zhang, Y Chang, W Cao, et al. Warm stamping technology of the medium manganese steel. Steel Res Int. 2018;89(9):1700360.

10. Jia Q, Liu L, Guo W, Peng Y, Zou G, Tian Z, et al. Microstructure and tensile-shear properties of resistance spot-welded medium Mn steel. Metals. 2018;8(1):48.

11. Wang Y, Ding K, Zhao B, Zhang Y, Wu G, Wei T, et al. Effect of the cooling time on the cross tensile strength of the resistance spot welded medium manganese steel. In: TMS 2020 149th Annual Meeting & Exhibition Supplemental; 2020; Pittsburgh, USA. Proceedings. Cham: Springer; 2020. p. 515-23.

12. Wang Y, Ding K, Zhao B, Zhang Y, Wu G, Wei T, et al. Highly enhanced cross tensile strength of the resistance spot welded medium manganese steel by optimized post-heating pulse. In: TMS 2020 149th Annual Meeting & Exhibition Supplemental; 2020; Pittsburgh, USA. Proceedings. Cham: Springer; 2020. p. 1871-80.

13. Cai ZH, Ding H, Misra RDK, Kong H, Wu HY. Unique impact of ferrite in influencing austenite stability and deformation behavior in a hot-rolled Fe–Mn–Al–C steel. Mater Sci Eng A. 2014;595:86-91.

14. Cai ZH, Ding H, Misra RDK, Ying ZY. Austenite stability and deformation behavior in a cold-rolled transformation-induced plasticity steel with medium manganese content. Acta Mater. 2015;84:229-36.

15. Maruyama H. X-ray measurement of retained austenite volume fraction. Jpn Soc Heat Treat. 1977;17:198-204.

16. Wang MM, Tasan CC, Ponge D, Raabe D. Spectral TRIP enables ductile 1.1 GPa martensite. Acta Mater. 2016;111:262-72.

17. Suh DW, Kim SJ. Medium Mn transformation-induced plasticity steels: recent progress and challenges. Scr Mater. 2017;126:63-7.

18. Han J, Silva AK, Ponge D, Raabe D, Lee S-M, Lee Y-K, et al. The effects of prior austenite grain boundaries and microstructural morphology on the impact toughness of intercritically annealed medium Mn steel. Acta Mater. 2017;122:199-206.

19. Pouranvari M, Marashi SPH. Critical review of automotive steels spot welding: process, structure and properties. Sci Technol Weld Join. 2013;18(5):361-403.

20. Pouranvari M, Khorramifar M, Marashi SPH. Ferritic–austenitic stainless steels dissimilar resistance spot welds: metallurgical and failure characteristics. Sci Technol Weld Join. 2016;21(6):438-45.

21. Saha DC, Ji CW, Park YD. Coating behaviour and nugget formation during resistance welding of hot forming steels. Sci Technol Weld Join. 2015;20(8):708-20.

22. Yuan X, Li C, Chen J, Li X, Liang X, Pan X. Resistance spot welding of dissimilar DP600 and DC54D steels. J Mater Process Technol. 2017;239:31-41.

23. Wang T, Hu J, Misra RDK. Microstructure evolution and strain behavior of a medium Mn TRIP/TWIP steel for excellent combination of strength and ductility. Mater Sci Eng A. 2019;753:99-108.

24. Han HN, Lee CG, Suh DW, Kim S-J. A microstructure-based analysis for transformation induced plasticity and mechanically induced martensitic transformation. Mater Sci Eng A. 2008;485(1-2):224-33.

25. Zhang H, Senkara J. Resistance welding: fundamentals and applications. Boca Raton: CRC Press; 2011.

26. Sajjadi-Nikoo S, Pouranvari M, Abedi A, Ghaderi AA. In situ postweld heat treatment of transformation induced plasticity steel resistance spot welds. Sci Technol Weld Join. 2018;23(1):71-8.

27. Pouranvari M, Marashi SPH. Factors affecting mechanical properties of resistance spot welds. Mater Sci Technol. 2010;26(9):1137-44.

28. Pouranvari M. Susceptibility to interfacial failure mode in similar and dissimilar resistance spot welds of DP600 dual phase steel and low carbon steel during cross-tension and tensile-shear loading conditions. Mater Sci Eng A. 2012;546:129-38.

29. Callister WD. Fundamentals of materials science and engineering. New York: John Wiley & Sons; 2001. 524 p.

30. Kazdal Zeytin H, Ertek Emre H, Kaçar R. Properties of resistance spot-welded TWIP steels. Metals. 2017;7(1):14.

31. Pouranvari M, Marashi SPH. Failure mode transition in AHSS resistance spot welds. Part I. Controlling factors. Mater Sci Eng A. 2011;528(29-30):8337-43.

32. Russo Spena P, De Maddis M, Lombardi F, Rossini M. Investigation on resistance spot welding of TWIP steel sheets. Steel Res Int. 2015;86(12):1480-9.